inventions

MDPI

Article

Mass Transfer Effects on the Mucus Fluid with Pulsatile Flow Influence of the Electromagnetic Field

Padmavathi Thiyagarajan [1], Senthamilselvi Sathiyamoorthy [1], Karuppusamy Loganathan [2,3,*], Oluwole Daniel Makinde [4] and Ioannis E. Sarris [5,*]

[1] Department of Mathematics, Vels Institute of Science, Technology & Advanced Studies, Vels University, Chennai 600117, India; padmavathi.phd@velsuniv.ac.in (P.T.); msselvi230@gmail.com (S.S.)
[2] Department of Mathematics and Statistics, Manipal University Jaipur, Jaipur 303007, India
[3] Research and Development Wing, Live4Research, Tiruppur 638106, India
[4] Faculty of Military Science, Stellenbosch University, Private Bag X1, Matieland 7602, South Africa; makinded@gmail.com
[5] Department of Mechanical Engineering, University of West Attica, 250 Thivon & P. Ralli Str., Egaleo, 12244 Athens, Greece
* Correspondence: loganathankaruppusamy304@gmail.com (K.L.); sarris@uniwa.gr (I.E.S.)

Abstract: The influence of pulsatile flow on the oscillatory motion of an incompressible conducting boundary layer mucus fluid flowing through porous media in a channel with elastic walls is investigated. The oscillatory flow is treated as a cyclical time-dependent flux. The Laplace transform method using the Womersley number is used to solve non-linear equations controlling the motion through porous media under the influence of an electromagnetic field. The theoretical pulsatile flow of two liquid phase concurrent fluid streams, one kinematic and the other viscoelastic, is investigated in this study. To extend the model for various physiological fluids, we postulate that the viscoelastic fluid has several distinct periods. We also apply our analytical findings to mucus and airflow in the airways, identifying the wavelength that increases dynamic mucus permeability. The microorganism's thickness, velocity, energy, molecular diffusion, skin friction, Nusselt number, Sherwood number, and Hartmann number are evaluated. Discussion is also supplied in various sections to investigate the mucosal flow process.

Keywords: COVID-19; electromagnetic force; mass transfer; mucus fluid; permeability; viscoelasticity

Citation: Thiyagarajan, P.; Sathiyamoorthy, S.; Loganathan, K.; Makinde, O.D.; Sarris, I.E. Mass Transfer Effects on the Mucus Fluid with Pulsatile Flow Influence of the Electromagnetic Field. *Inventions* **2022**, *7*, 50. https://doi.org/10.3390/inventions7030050

Academic Editors: Goshtasp Cheraghian and Dimitris Drikakis

Received: 20 April 2022
Accepted: 21 June 2022
Published: 24 June 2022

1. Introduction

We're still in the midst of a tremendous phase of susceptibility and risk brought on by SARS-CoV-2 transmission and eventual COVID-19 illness. The emergence of a combination of mass components between one region to another is called a mass exchange. This interaction occurs in various associations to achieve a service that meets the needs of cycles, including retention, dissipation, refinement, and so on. This connection promotes mucus layer production and reduces the energy required to keep the tissue functioning perfectly. The human respiratory organ delivers mucous fluid. The physical fluid structure varies depending on its motivation and the area of the body where it is present. Mucin, a chemical produced by the body, is used to make every mucus; however, water makes up 90% of bodily fluid. The mucus gel is primarily smooth and exact. The average adult produces between 1 and 1.5 quarts of body fluid daily. The respiratory system contains most of it, including the mouth, throat, nose, and lungs. The mucous fluid in our lungs can help to eliminate bacteria that could cause infection in one way or another. Infections, tiny organisms, and allergies can all be prevented by nasal mucus. While elastic components occur, the dynamical penetration reflects resonant frequency and specific cardiac drag force patterns that maximize fluid velocity amplitude. Mucus distribution and velocity are studied in terms of pulmonary circulation and passage, particularly gas transportation

under different phases of oxygenation, chemical transport, and lubricant interactions in the terminal lungs.

Pablo Alberto de la Guerra et al. [1] studied the pulsatile movement of bicontinuous parallels fluid streams, with one being Newtonian and the other being viscoelastic. Under a single framework, the influence of chemical process, heat, and mass transfer on the oscillating magnetohydrodynamic flow of blood was studied by Misra et al. [2], with blood being treated as a second-grade fluid. Patel and Birla [3] focused on constructing a peristaltic circulation biosensor and measured the construct's ability to handle and produce pressure as well as the impact of the biomechanical condition on structure performance. In Sara et al.'s [4] study, the Jeffrey viscoelastic model is utilized to reproduce non-Newtonian attributes.

Zeinab Abbasi et al. [5] also examined each reduced-order model's applications and limits. This model begins from an exact multi-stretching model of leading and respiratory aviation routes (i.e., the base model); they recommend an intermediary model directing aviation routes and a diminished request model of respiratory aviation routes in light of the base model to decrease computational expense while holding the precision essentially. There are a couple of studies by Kori et al. [6–8] that thought about the lung as a porous medium; they anticipated that penetration could be comparable to porosity or constant. The impact of intermittent porousness on the two-layered pulsatile streams of gooey air coursing through aviation route generations 5–10 was related to occasional inhaling. Veera Krishna et al. [9] considered blood's unstable two-layered Magnetohydrodynamics (MHD) oscillatory progression in a permeable arteriole affected by a uniform cross-over attractive field in a planar region; intensity and mass exchange during blood vessel blood movement through a porous medium was also investigated. In the study by Akbar et al. [10], an extensive range of situations have been explored in peristaltic transport with micropolar liquids and, independently, other rheological streams with cilia impacts. No review has thus far concentrated on the consolidated micropolar peristaltic drive with cilia beating effects.

Ma et al. [11] introduced modern advances in the planning of nanodrug conveyance frameworks and transporter-free medication conveyance microfluidic frameworks, as well as the development of in vitro models on a chip for drug proficiency assessment of medication conveyance frameworks. A hypothetical study of a rheological liquid suspended with two kinds of nanoparticles through a lofty direction is introduced by Mubbashar Nazeer et al. [12] and Ramesh et al. [13]. A theoretical study is conducted on magnetohydrodynamic pumping of electroconductive couple stress physiological liquids (e.g., blood) over a two-dimensional ciliated channel. In Sedaghat et al.'s [14] study, a mathematical strategy in light of the Lattice Boltzmann technique displays viscoelastic liquid collaboration complex limits, which are regularly seen in natural frameworks and modern practices. Then, the strategy is applied to reproduce the mucociliary transport interaction of the human respiratory framework.

Under the effects of momentum and thermal slip, Munwar et al. [15] examined a ciliated channel coated by Prandtl fluid, a visco-inelastic fluid, and containing the Hartmann layer. Fluid flow in the conduit is generated through cilia whippings that maintain an elliptic path throughout the flow direction. An entropy examination of the flow was also conducted in the wave frame. The mechanical flow of the biomolecule through some homogeneous conduit was studied by Nazeer et al. [16]. Couple stress nanofluid flow is mainly caused by metachronal waves created by the ciliary movement of flagellated components.

Mukhopadhyay et al. [17] investigated a mathematical mass transfer model of blood flow under stenotic scenarios. The Carreau fluid model classifies circulating blood as a non-Newtonian fluid, with the vessel wall being thought of as flexible. A non-Newtonian biofluid's pulsatile hydromagnetic flow and heat transmission through a saturated non-Darcian poroelastic channel with viscous heating were investigated by Rawat et al. [18]. Mucus excretion inside the airways is a physiological way to safeguard the lungs by absorbing and expelling inhaled persistent materials via the mucociliary elevator [19]. Globally, infectious diseases are a significant cause of morbidity and mortality. Malaria,

TB, and viral hepatitis contamination are exceptionally hard to treat, as they are constantly propagating and have low survival percentages [20]. Mucosal tissue is generated by goblet cells in the membrane of mucosal surfaces of the lungs. Microbes congregate on a surface and create an extracellular matrix of large polysaccharides (such as glycerin and N-acetyl glycine), DNA, and proteins known as a swarm. Singh et al. [21] established a worldview about smoke-related inward breath poisonousness testing in vitro and a concise outline of breathing LOC trial plan ideas. One of the most complicated living organisms is the human respiratory system. Conversely, each lung bronchial can be modeled as a tubular elastic conduit (up to a certain macroscopic level). Padmavathi et al. [22] tried to manifest on combined convection flow of pleural and mucus fluid influenced by injection.

This paper investigates the theoretical pulsatile flow of two liquid phase concurrent fluid streams, with one being a kinematic fluid and the other a viscoelastic fluid. We consider that the viscoelastic fluid has numerous characteristic periods to extend the model for various body fluids. The viscoelastic fluid is believed to have countless functional times. In the time−frequency, we propose a generalized Darcy's law. Furthermore, we extend our analytical findings to mucus and airflow in the airways, discovering the wavelength that promotes dynamic mucus permeability. It is expected that the current review will help survey the accuracy of the information presented through examinations of these various lung disorders. Significant mucus dispersion is essential for optimal airway removal and healthy respiratory system activity.

2. Formulation of the Problem

Three-dimensional spherical vessels make up the majority of the circulatory system. Blood motion can be approximated as channel flow in some circumstances, such as in micro vessels of the lungs. Taking this and many other rational and logical investigations into account, Cartesian coordinates are used. The flow is symmetrical about the channel's axis and is propelled by the squeezing of the flow path, with each wall's velocity corresponding to the axial coordinate. To examine the second-order consequences of unsteady MHD blood flow, consider the fluid motion of a second-order fluid between two parallel plates at $y \to 0$ and $y \to \infty$. The microscopic, motile ciliary movement of the hierarchically arranged biological flow is performed by spreading metachronal waves with a constant speed c on the opposing walls; a time-dependent pressure gradient is involved and a Boussinesq approximation is applied over the mucus layer model. It can be found in Figure 1.

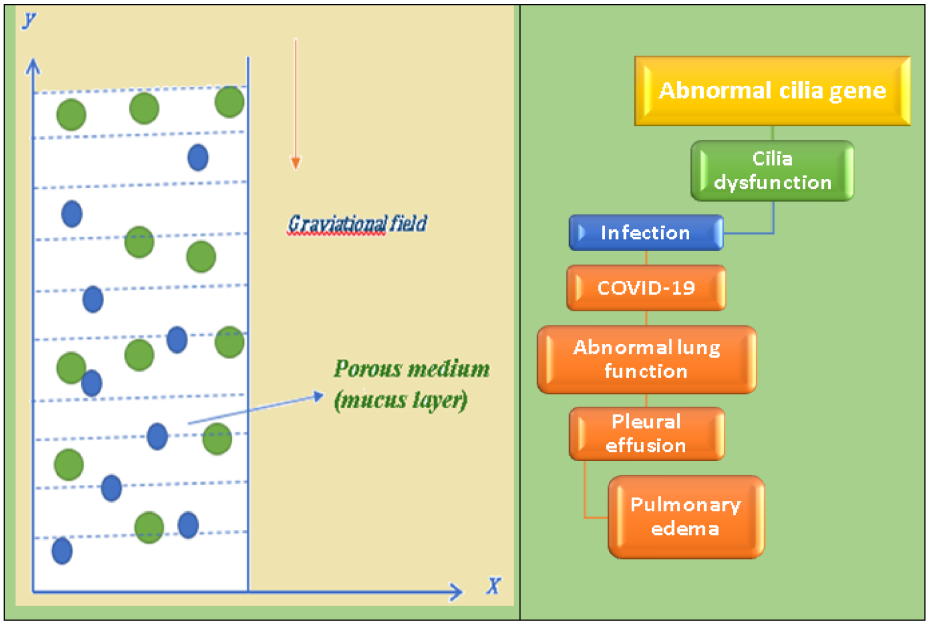

Figure 1. Multiple lung disorders arrangement and flow geometry.

In the structure, the mass, speed, energy, and mass diffusivity conditions were reported by Misra et al. [2].

Mass conservation:

$$\frac{\partial {v_m}^*}{\partial y^*} = 0 \tag{1}$$

Momentum conservation:

$$\frac{\partial {u_m}^*}{\partial t^*} = -\frac{1}{\rho}\frac{\partial {P_m}^*}{\partial t^*} + \nu\left(\frac{\partial^2 {u_m}^*}{\partial {y^*}^2}\right) + g\beta_T({T_m}^* - {T_\infty}^*) + g\beta_C({C_m}^* - {C_\infty}^*) - \frac{\nu}{{k_m}^*}{u_m}^* - \frac{\sigma {B_0}^2 {u_m}^*}{\rho} \tag{2}$$

Energy Conservation:

$$\left(\frac{\partial {T_m}^*}{\partial t^*}\right) = \frac{k_T}{\rho C_p}\left(\frac{\partial^2 m^*}{\partial {y^*}^2}\right) - J({T_m}^* - {T_\infty}^*) \tag{3}$$

Concentration Conservation:

$$\left(\frac{\partial {C_m}^*}{\partial t^*}\right) = D\left(\frac{\partial^2 {C_m}^*}{\partial {y^*}^2}\right) \tag{4}$$

$$\begin{gathered} {u_m}^* = 0\,,\ {C_m}^* = {C_\infty}^* \ and\ {T_m}^* = {T_\infty}^*\ for\ y^* \geq 0, x^* > 0, \quad t^* \leq 0 \\ {u_m}^* = h\ Cos\omega t^*\,,\ {C_m}^* = {C_w}^* and\ {T_c}^* = {T_w}^*\ at\ y^* = 0 \\ {u_m}^* = 0,\ {C_m}^* \to {C_\infty}^*\ and\ {T_m}^* = {T_\infty}^*\ at\ y^* \to \infty\ t > 0 \end{gathered} \tag{5}$$

The nomenclature defines all parameters. It's important to begin with dimensionless quantities, which are classified as follows:

$$\begin{gathered} u_m = \tfrac{{u_m}^*}{U_0},\ x = \tfrac{x^*}{h_m}, y = \tfrac{y^* U_0}{\nu},\ {\theta_m}^* = \tfrac{{T_m}^* - {T_\infty}^*}{{T_w}^* - {T_\infty}^*}\,, \\ {\phi_m}^* = \tfrac{{C_m}^* - {C_\infty}^*}{{C_w}^* - {C_\infty}^*}\,, P = \tfrac{{P_m}^*}{\rho {u_0}^2} t = \tfrac{t^* {v_0}^2}{\nu}\,,\ \propto^2 = \tfrac{\omega l^2}{\nu} \end{gathered} \tag{6}$$

where ${\theta_m}^*$and C^* are dimensionless.

Temperature and Concentration for mucus fluid flow:

$$\begin{gathered} \tfrac{\partial u_m}{\partial t} = -\tfrac{\partial P}{\partial x} + \left(\tfrac{\partial^2 u_m}{\partial y^2}\right) - \sigma^2 u_m - M u_m + \tfrac{G}{Re^2} u_m + Gr\theta_m + Gc\phi_m - \tfrac{\partial P}{\partial x} = e^{-\lambda t} \\ \tfrac{\partial u_m}{\partial t} = e^{-\lambda t} + \left(\tfrac{\partial^2 u_m}{\partial y^2}\right) - \sigma^2 u_m + Gr\theta_m + Gc\phi_m \end{gathered} \tag{7}$$

$$\frac{\partial \theta_m}{\partial t} = \frac{1}{Pr}\frac{\partial^2 \theta_m}{\partial y^2} - J\theta_c \tag{8}$$

$$\frac{\partial \phi_m}{\partial t} = \frac{1}{Sc}\frac{\partial^2 \phi_m}{\partial y^2} \tag{9}$$

where

$$Gr = \frac{g\beta_T({T_w}^* - {T_\infty}^*)\nu}{{U_0}^3}\ [\text{Grashof number}]$$

$$Gr = \frac{g\beta_C({C_w}^* - {C_\infty}^*)\nu}{{U_0}^3}\ [\text{Mass Grashof number}]$$

$$\sigma^2 = \frac{\nu^2}{{U_0}^2 K}\ [\text{Porosity Parameter}];\ \text{R}e = \frac{h u_m}{\nu}\ [\text{Reynolds Number}]$$

$$Pr = \frac{\mu C_p}{k_T}\ [\text{Prandtl number}];\ G = \frac{R\ N\ h^2}{\mu}\ [\text{Particle mass Number}]$$

$$M = \frac{\sigma {B_0}^2\ \mu}{{U_0}^2}\ [\text{Hartmann Number}]$$

The substitution of limit conditions are:

$$\begin{gathered} u_m = 0 \; as \; y \to \infty \\ u_m = Cos \propto^2 t \; as \; y \to 0 \\ \theta_m = 0 \; at \; y \geq 0, \phi_m = 0 \; at \; y \geq 0 \\ \theta_m = 0 \; , \; \phi_m = 0 \; as \; y \to \infty \\ \theta_m = 1 \; , \phi_m = 1 \; as \; y = 0 \end{gathered} \tag{10}$$

3. Method of Solution

The standard Laplace technique and its inverse transformations are used to solve the mathematical model generated and specified by Equations (7)–(9) and boundary conditions by Equation (10). The following transformations are used in MATLAB software to find solutions for the mucus fluid velocity, temperature, and concentration functions:

$$L(\theta_m) = \frac{e^{-y\sqrt{(J+s)\mathrm{Pr}}}}{s} \tag{11}$$

$$L(\phi_m) = \frac{e^{-y\sqrt{s(Sc)}}}{s} \tag{12}$$

$$\begin{gathered} L(u_m) = e^{-y\sqrt{k+s}}\left[\frac{s}{s^2+\beta^2} - \frac{1}{k+\lambda}\left[\frac{1}{s-k} - \frac{1}{s+\lambda}\right] + \frac{Gr}{R}\left[\frac{1}{s} + \frac{1-pr}{R-s(pr-1)}\right]\right] - \frac{Gm}{k}\left[\frac{1}{s} + \frac{sc-1}{k-s(sc-1)}\right] + \frac{1}{k+\lambda}\left[\frac{1}{s-k} - \frac{1}{s+\lambda}\right] - \\ \frac{Gr}{R}\left[\frac{e^{-y\sqrt{(J+s)pr}}}{s} - \frac{(1-pr)e^{-y\sqrt{(J+s)pr}}}{R+s(pr-1)}\right] + \frac{Gm}{k}\left[\left[\frac{e^{-y\sqrt{S\ Sc}}}{s} - \frac{(sc-1)e^{-y\sqrt{S\ Sc}}}{k-s(sc-1)}\right]\right] \end{gathered} \tag{13}$$

Appendix A contains the definitions of a few variables that we will require for future work.

Inverse Laplace:

$$\theta_m = \frac{1}{2}\left\{\left[e^{\mp y\ Pr\sqrt{J}}\left[erfc\left(\eta\sqrt{Pr}\right) \mp \sqrt{JPrt}\right]\right]\right\} \tag{14}$$

$$\phi_m = erfc\left(\eta\sqrt{Sc}\right) \tag{15}$$

$$\begin{gathered} u_m = Cos\ \beta\left(t - \sqrt{k+s}\right) - \frac{1}{k+\lambda}e^{k(t-\sqrt{k+s})} + \frac{1}{k+\lambda}e^{-\lambda(t-\sqrt{k+s})} \\ + \left[\frac{Gr}{R} - \frac{Gm}{2k}\right]\left[e^{\mp y\sqrt{k}}erfc\left(\eta \mp \sqrt{kt}\right)\right] \\ - \frac{Gre^{Qt}}{2}\left[e^{\mp y\sqrt{Q+k}}erfc\left(\eta \mp \sqrt{(Q+k)t}\right)\right] \\ - \frac{Gm\ e^{-Dt}}{2k}\left[e^{\mp y\sqrt{k-D}}erfc\left(\eta \mp \sqrt{(k-D)t}\right)\right] \\ + \frac{1}{k+\lambda}\left(e^{kt} - e^{-\lambda t}\right) - \frac{Gr}{2R}\left[e^{\mp y\ Pr\sqrt{J}}\left[erfc\left[\left(\eta\sqrt{Pr}\right) \mp \sqrt{JPr\ t}\right]\right]\right] \\ + \frac{Gre^{Qt}}{2R}\left[e^{\mp y\ Pr\sqrt{J+Q}}\left[erfc\left[\left(\eta\sqrt{Pr}\right) \mp \sqrt{(J+Q)\mathrm{Pr}t}\right]\right]\right] \\ + \frac{Gm}{k}\left[erfc\left(\eta\sqrt{Sc}\right) - e^{D-(t-\sqrt{Sc\ S})}\right] \end{gathered} \tag{16}$$

$$Q = \frac{R}{Pr-1}, \;\; D = \frac{k}{Sc-1}, \;\; \beta = \alpha^2, \; R = (J\ Pr - k), \; k = \sigma^2 + M, \eta = \frac{y}{2\sqrt{t}}$$

Skin Friction:

$$\begin{gathered} \tau = \left[\frac{\partial u_m}{\partial y}\right]_{y=0} = \left[\frac{\partial u_m}{\partial \eta}\right]_{\eta=0} = \left(-\frac{\mathrm{Gm}}{2k} + \frac{\mathrm{Gr}}{R}\right)\left(-\frac{4e^{-kt}}{\sqrt{\pi}} - 2\sqrt{k}\sqrt{t}\ \mathrm{erfc}\left[-\sqrt{kt}\right] + 2\sqrt{k}\sqrt{t}\ \mathrm{erfc}\left[\sqrt{kt}\right]\right) - \\ \frac{1}{2}e^{Qt}\mathrm{Gr}\left(-\frac{4e^{-(k+Q)t}}{\sqrt{\pi}} - 2\sqrt{k+Q}\sqrt{t}\ \mathrm{erfc}\left[-\sqrt{(k+Q)t}\right] + 2\sqrt{k+Q}\sqrt{t}\ \mathrm{erfc}\left[\sqrt{(k+Q)t}\right]\right) - \\ \frac{1}{2k}e^{-dt}\mathrm{Gm}\left(-\frac{4e^{-(-D+k)t}}{\sqrt{\pi}} - 2\sqrt{-D+k}\sqrt{t}\ \mathrm{erfc}\left[-\sqrt{(-D+k)t}\right] + 2\sqrt{-D+k}\sqrt{t}\ \mathrm{erfc}\left[\sqrt{(-D+k)t}\right]\right) - \\ \frac{\mathrm{Gr}\left(-\frac{4e^{-J\mathrm{Pr}t}\sqrt{\mathrm{Pr}}}{\sqrt{\pi}} - 2\sqrt{J}\mathrm{Pr}\sqrt{t}\ \mathrm{erfc}\left[-\sqrt{J\mathrm{Pr}t}\right] + 2\sqrt{J}\mathrm{Pr}\sqrt{t}\ \mathrm{erfc}\left[\sqrt{J\mathrm{Pr}t}\right]\right)}{2R} - \frac{2e^{-Qt-\mathrm{Pr}(J+Q)t}\mathrm{Gr}\sqrt{\mathrm{Pr}}}{\sqrt{\pi}R} - \frac{2e^{-Qt}\mathrm{GrPr}\sqrt{J+Q}\sqrt{t}\ \mathrm{erfc}\left[-\sqrt{\mathrm{Pr}(J+Q)t}\right]}{R} - \frac{2\mathrm{Gm}\sqrt{\mathrm{Sc}}}{M\sqrt{\pi}} \end{gathered} \tag{17}$$

Nusselt Number:

$$Nu = \left[\frac{\partial \theta_m}{\partial y}\right]_{y=0} = \left[\frac{\partial \theta_m}{\partial \eta}\right]_{\eta=0} = -\frac{2e^{-JPrt}\sqrt{Pr}}{\sqrt{\pi}} - \frac{e^{-JPrt}\sqrt{Pr}}{2\sqrt{\pi}\sqrt{t}} - \frac{1}{2}eErfc\left[-\sqrt{JPrt}\right] - 2\sqrt{JPr}\sqrt{t}\,erfc\left[-\sqrt{JPrt}\right] \quad (18)$$

Sherwood number:

$$Sh = \left[\frac{\partial C_m}{\partial y}\right]_{y=0} = \left[\frac{\partial C_m}{\partial \eta}\right]_{\eta=0} = -\frac{\sqrt{SC}}{\sqrt{\pi}\sqrt{t}} \quad (19)$$

4. Results and Discussion

The purpose of this research was to examine the influence of heat and mass transfer in the presence of a magnetic field in a respiratory fluid flow while accounting for velocity slip and second-grade effects. The following values of the various parameters involved in the analytical analysis have been used for numerical computation.

The advantage of using the Laplace transform technique [23] is that it converts an ODE into a logarithmic condition of a comparable procedure that is easier to handle, despite the fact that it is a component of a compound variable. This strategy's primary advantage is that it is characterized by a mixture of steady and erratic motion.

When a magnetic effect occurs, these values/ranges of the parameters are mostly reflective of bodily fluid flow. The analytical formulas derived in the previous part have been computed using these data and suitable software, namely MATLAB.

Figure 2 depicts the effect of the porosity parameter on the velocity profile in the general magnetorheological situation. Because the Darcy parameter is related to permeability, an increase in conductivity implies an increase in permeability. Consequently, the amount of matrix particles in the porous media diminishes. In biomedical scenarios, such threads can take the form of blocking material, tumors, or fatty deposits. A reduced presence of such elements will result in a drop in the Darcian drag force in Equation (2), lowering the resistance to flow and accelerating the biofluid, increasing velocity U.

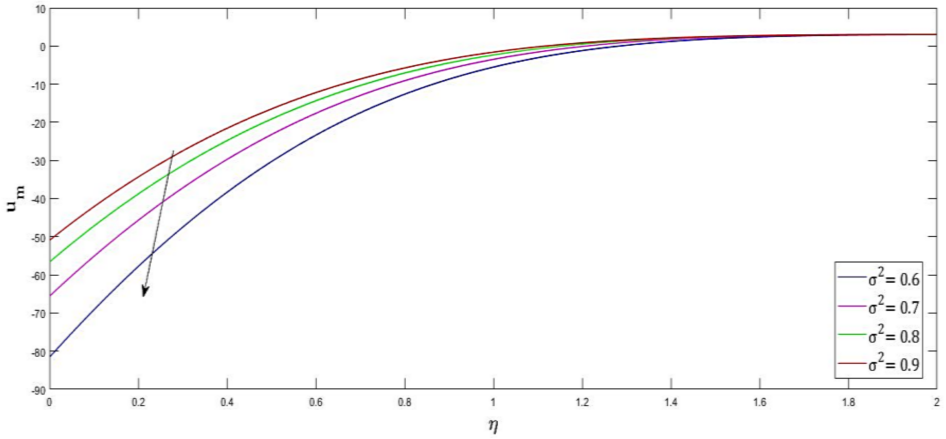

Figure 2. Variation in velocity profile with respect to porosity parameter.

Figure 3 shows that speed goes up as the Hartmann number increases. It is then expected that an expansion in M improves the resistive power, called the Lorentz force, which goes against the level stream. The consequences of the hydrodynamic case and its related issues can be recuperated as a restricting instance of our investigation by taking M = 0.

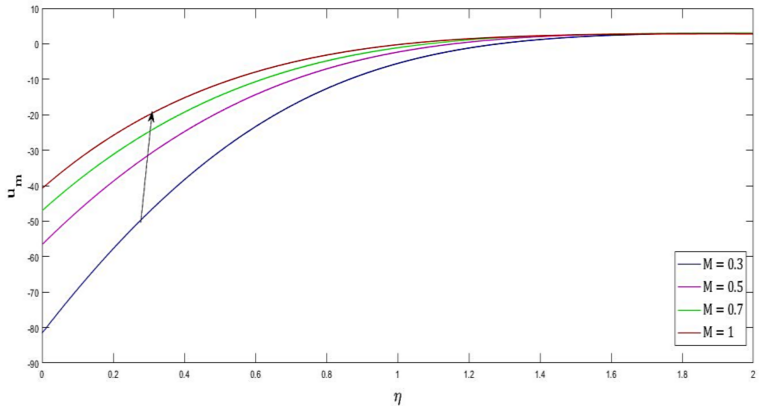

Figure 3. Variation in velocity profile with respect to Hartmann number.

Figure 4 depicts the effect of the Grashof number Gr for the heat transfer on the velocity U of the flow field. In physical terms, the Grashof number for the thermal performance Gr denotes the strength of the thermal buoyancy force compared to the viscous hydrodynamic force in the boundary layer. The Grashof number Gr for the heat transfer accelerates the velocity U of the flow field at all sites, according to the curves. The reason for this is that the thermal buoyancy force has increased. Figure 5 shows the influence of the Grashof number Gm for the molecular diffusion on the flow field's velocity U. Grashof number Gm for mass transfer represents the strength of a species' buoyant force in proportion to viscous hydrodynamic force.

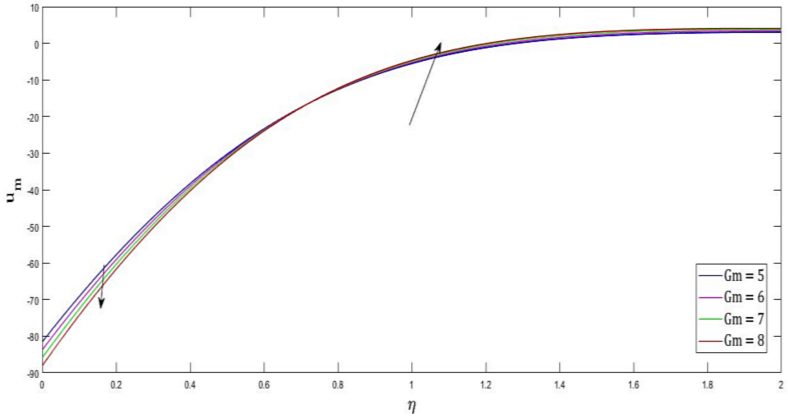

Figure 4. Variation in velocity profile with respect to mass Grashof number.

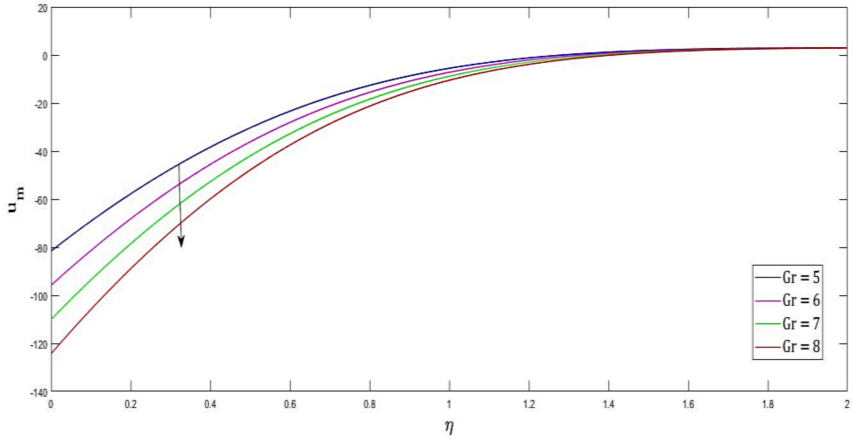

Figure 5. Variation in velocity profile with respect to mass Grashof number.

Figure 6 shows the influence of heat absorption. This finding is based on the heat absorption parameters, J = 0.6, 0.7, 0.8, and 0.9. The observation is documented for parallel surfaces. We discovered that the JF temperature is a declining function of the heat absorption parameter in the domain. This is because fluctuations in J represent a loss of latent heat, which causes the Jeffrey fluid temperature to drop in the flow pattern [24]. The hypothesis of temperature effects resulted in the creation of the heat transfer parameter. It's important to remember that higher thermal conductivity can lead to an overflow of the thermal boundary layer. This phenomenon could be controlled by deploying a heat sink to reduce the heat and a heat source to raise its temperature to the maximum required level. Figures 7 and 8 show the decrease in temperature profiles for various Prandtl numbers and time. For = 15, the peak velocity drops to around 0.9.

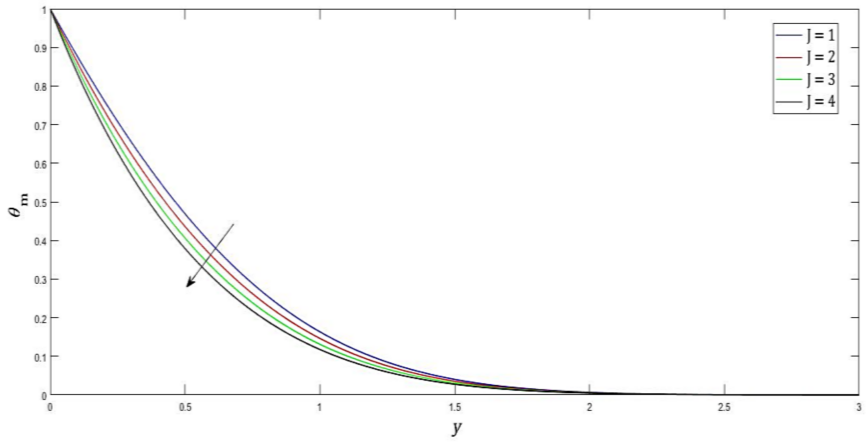

Figure 6. Variation in temperature profile with respect to heat absorption parameter.

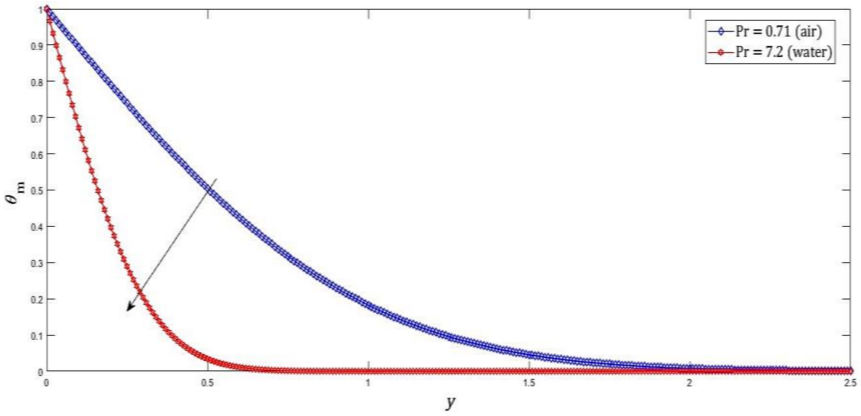

Figure 7. Variation in temperature profile with respect to Prandtl number.

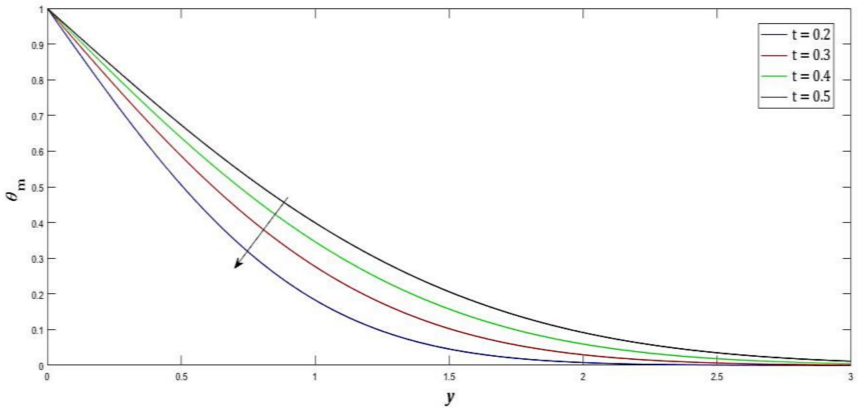

Figure 8. Variation in temperature profile with respect to time.

In Figure 9, the mass transfer equivalent of the Prandtl number is the Schmidt number. Sc and Pr have identical values (0.7) for gases, which is utilized to create simple forced convection heat transit equivalents. For frequencies somewhere in the range of 10^{-4} and 10^2 Hz, the typical consistent shear thickness fluctuates, crossing thickness values as high as $10^3\ Pa-s$ and as low as $10^2\ Pa-s$. Human bodily fluid has a consistency of 10^4–10^6 times that of water when sheared at unassuming shear rates. The rise in Sc causes the concentration boundary layer to be smaller than the momentum boundary layer, as shown above. In Figure 10, the concentration profile increased in a time-dependent manner.

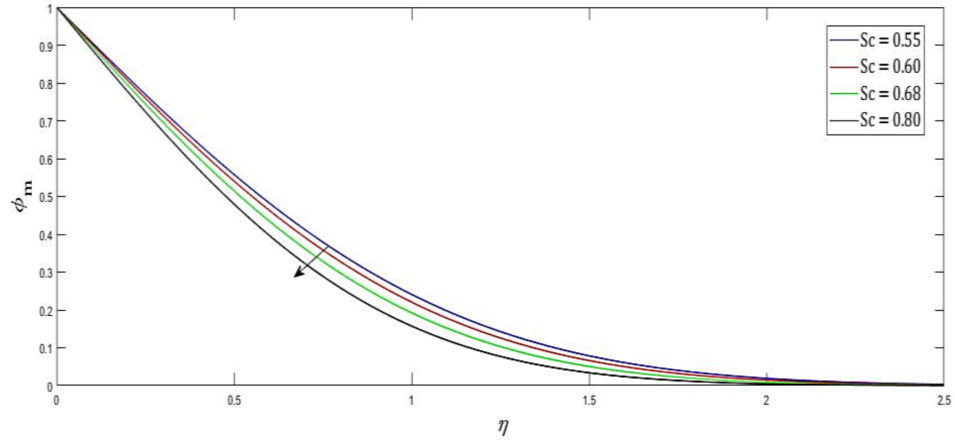

Figure 9. Variation in concentration profile with respect to Schmidt number.

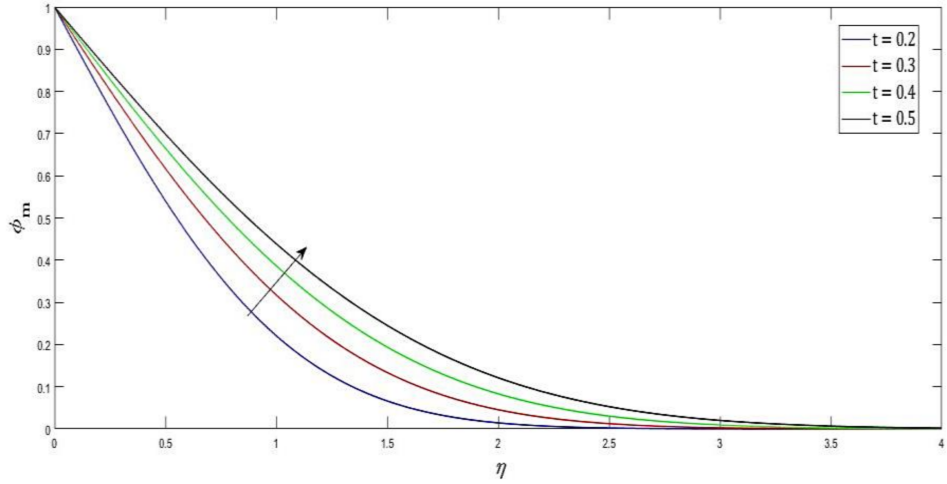

Figure 10. Variation in concentration profile with respect to time.

We present one representation of pulsatile airflow frequency in proportion to viscous effects. Figure 11 shows that increasing the Womersley number increases the mucus fluid velocity profile. At the level of the terminal courses, it is worth noting that Womersley numbers tend to one. Womersley numbers in capillaries, veins, and venules are less than one. The stagnation force is less substantial in these areas and the tension angle is still up in the air because of the balancing among thick weights and the pressure inclination. This is referred to as the microcirculation. Tabassum Naz Sindhu et al. [25] discussed a straight representation of the thickness work.

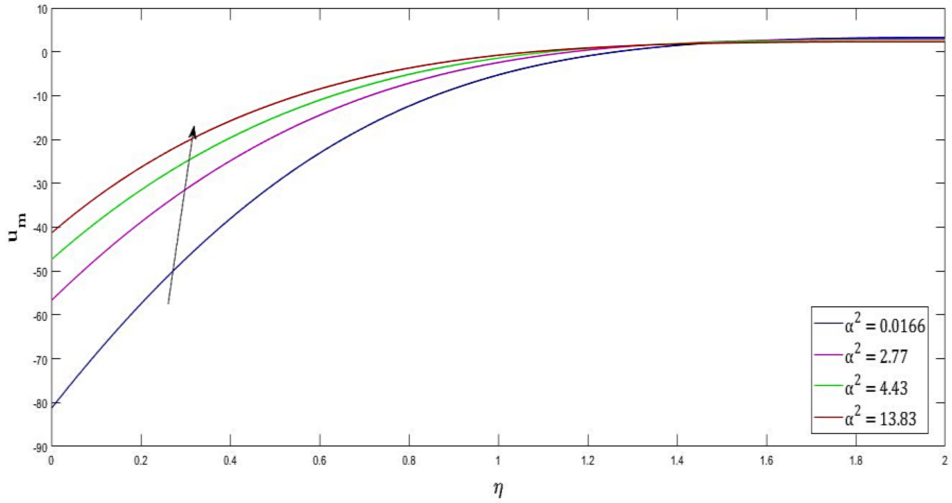

Figure 11. Variation in velocity profile with respect to Womersley number.

Non-Newtonian fluids, on the other hand, are thought to be more appropriate for heat mass transport than Newtonian fluids, notably in medical sciences where medication therapy is concerned. Numerical qualities of the combination of the Lindley model with two parts (2-CMLM) are examined by Anum Shafiq et al. [26].

For both water $(Pr = 7.0)$ and air $(Pr = 0.71)$, the Nusselt number rises with expanding values of Pr. Figure 12 shows that the Nusselt number for water is higher than that of air. This is because for small Pr values, gains are equivalent to increasing heat strength. Thus, heat can disperse away from the periciliary layer more quickly than larger Pr values, slowing the heat exchange. On the other hand, the diffusion thermal efficiency has the inverse result on the Nusselt number and temperature profile. The Sherwood number stagnation is displayed in Figure 13 by the expanding values of $Sc.Sh < 1$; this indicates that the PCL's pseudo-diffusivity is weaker than the substance's molecular diffusivity.

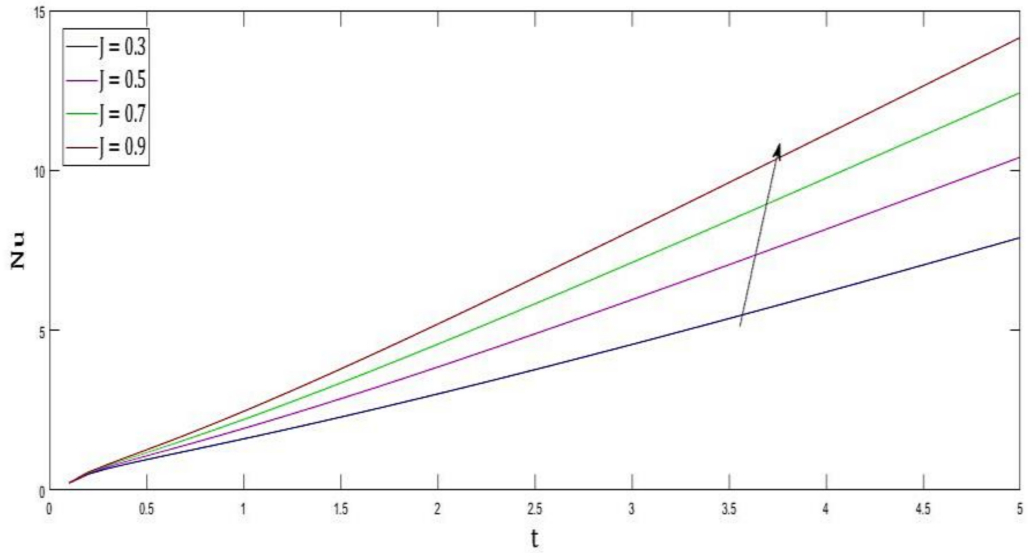

Figure 12. Variation in Nusselt number with respect to heat absorption parameter.

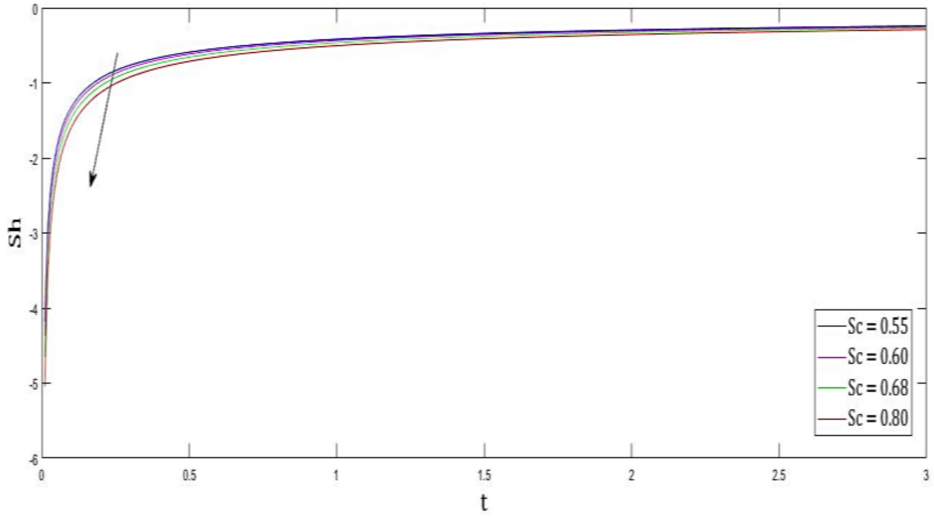

Figure 13. Variation in Sherwood number with respect to Schmidt number.

The potential numerical gains of skin friction τ are presented in Figures 14 and 15 for different thermal and mass Grashof numbers. Moreover, it is seen that the skin friction is augmented with increasing potential gains of the thermal and mass Grashof number.

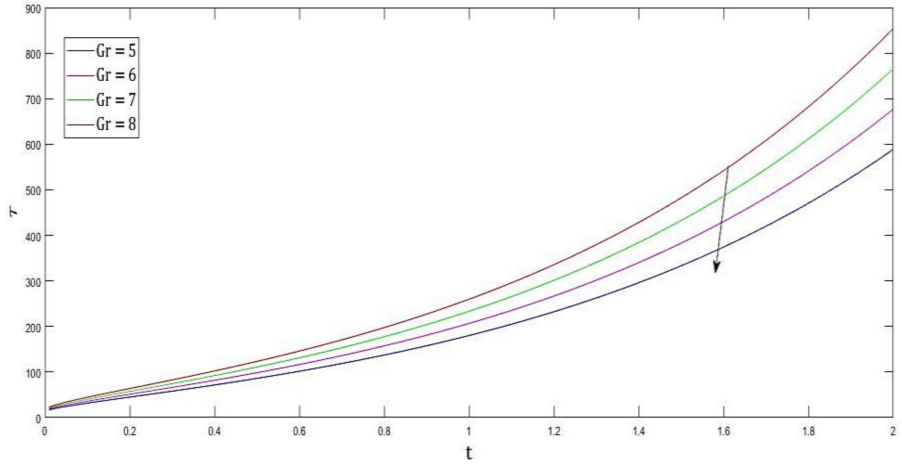

Figure 14. Variation in skin friction with respect to Grashof number.

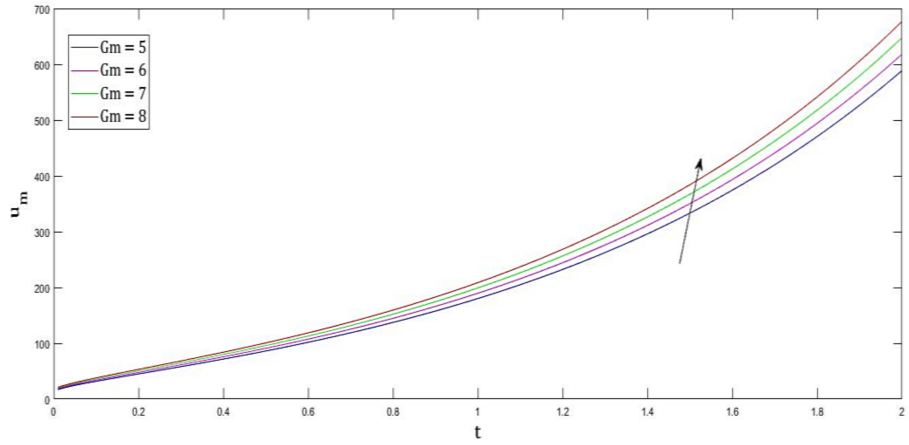

Figure 15. Variation in skin friction with respect to mass Grashof number.

5. Conclusions

The impact of magnetic effects and mass and energy transport on the magnetohydrodynamic oscillatory flow of mucus fluid is studied using a novel model. The periodic expulsion of mucus into the capillary system by the physical beating function of the chest is responsible for the pulsatility of mucociliary clearance.

The current findings have important implications for movement in tiny passageways such as the alveoli, where the red cell diameter is greater than the pore length. It contributes some knowledge toward understanding the pathophysiological conditions of the throbbing mucus fluid stream in a limited porous region, considering the impacts, for example, outside the attractive field and intensity transfer. Fluid dynamicists and physiologists working on blood flow in the presence of a magnetic field should be fascinated by the data presented here.

The final reports of the review produce the accompanying outcomes:

1. Velocity profile increases as porosity, thermal, and mass Grashof number increases.
2. Temperature profile decreases as J, and Pr diminishes.
3. Concentration profile increases as Sc increases.
4. Sherwood's Nusselt number rises as Pr values broaden. With the expanding values of Sc, the number grows.

Enault et al. [27] stated that force dissemination is the predominant impact. It has been proven that the momentum diffusion operator is exceedingly stiff. Sufficient time integrators, for example, dramatic integrators, will be utilized in the future to limit the computational season of force dissemination. The dominant input parameter is the epithelium cilia displacement. Accurate computation of epithelium dynamics will be required in order to get correct bottom boundary conditions for mucus. The mechanical properties of cilia will also be investigated. Furthermore, although this research was considered to be kinematic for expediency, the mucus rheological framework needs to be modified to account for viscoelasticity and hydration level.

Author Contributions: Conceptualization, P.T. and K.L. and O.D.M.; methodology, P.T.; software, P.T. and S.S.; validation, P.T., S.S. and K.L.; formal analysis, S.S. and K.L.; investigation, S.S. and I.E.S.; resources, P.T. and S.S.; data curation, O.D.M.; writing—original draft preparation, P.T.; writing—review and editing, K.L.; visualization, P.T. and I.E.S.; supervision, S.S. and K.L.; project administration, I.E.S.; funding acquisition, K.L. and I.E.S. All authors have read and agreed to the published version of the manuscript.

Funding: This research received no external funding.

Institutional Review Board Statement: Not applicable.

Informed Consent Statement: Not applicable.

Data Availability Statement: Not applicable.

Acknowledgments: We are extremely thankful to the supervisor and fair-minded mediator for their judicious translation and suggestion, which refined the excellency of this original manuscript.

Conflicts of Interest: The authors declare no conflict of interest.

Nomenclature

u_m , v_m	dimensionless velocity components for mucus fluid in x* and y*directions $\left[\frac{m}{s}\right]$
u_m* , v_m*	dimensional velocity components for mucus fluid flow in x and y direction
ρ	Fluid density $[Kg/m^3]$
ν	Kinematic viscosity $\left[m^2/s\right]$
μ	Dynamic viscosity [Pa s] (or) $\left[N\,s/m^2\right]$
k_m*	Permeabilty of porous layer (mucus layer) $\left[m^2\right]$
p	Pressure [Pa]

U_0	Characteristic velocity [m/s]
α^2	Womersely number
λ	Oscillating parameter
c_p	Specific heat capacity at constant pressure [J/kg/K]
T_w	Wall temperature of mucus fluid [°C or K]
C_w	Wall concentration of mucus fluid flow
T	Ambient temperature of mucus fluid flow [°C or K]
C_0	Ambient concentration of mucus fluid flow
Re	Reynolds number
J	Heat conduction parameter $\left[\frac{kg}{m^3}/s\right]$
K_T	Thermal conductivity [W/m/K]
t	Dimensionless time [second]
D	Mass diffusivity $[m^2/s]$
σ^2	Permeability parameter
g	Acceleration due to gravity $[m/s^2]$
Gc	Grashof number for mass transfer
Gr	Grashof number for heat transfer
Pr	Prandtl number
Sc	Schmidt number
θ	Temperature [°C or K]
C	Transport diffusivity of the fluid
x and y	Cartesian coordinates

Appendix A

$$Q = \frac{R}{Pr-1},\ D = \frac{k}{Sc-1},\ \beta = \alpha^2,\ R = (J\ Pr - k),\ k = \sigma^2 + M, \eta = \frac{y}{2\sqrt{t}}$$

References

1. De la Guerra, P.A.; Poiré, E.C. Pulsatile parallel flow of air and a viscoelastic fluid with multiple characteristic times. An application to mucus in the trachea and the frequency of cough. *J. Phys. Condens. Matter.* **2022**, *34*, 35561687. [CrossRef]
2. Misra, J.; Adhikary, S. MHD oscillatory channel flow, heat and mass transfer in a physiological fluid in presence of chemical reaction. *Alex. Eng. J.* **2016**, *55*, 287–297. [CrossRef]
3. Patel, N.M.; Birla, R.K. Pulsatile flow conditioning of three-dimensional bioengineered cardiac ventricle. *Biofabrication* **2017**, *9*, 015003. [CrossRef] [PubMed]
4. Abdelsalam, S.I.; Bhatti, M.M.; Zeeshan, A.; Riaz, A.; Bég, O.A. Metachronal propulsion of a magnetised particle-fluid suspension in a ciliated channel with heat and mass transfer. *Phys. Scr.* **2019**, *94*, 115301. [CrossRef]
5. Abbasi, Z.; Boozarjomehry, R.B. Various reduced-order surrogate models for fluid flow and mass transfer in human bronchial tree. *Biomech. Model. Mechanobiol.* **2021**, *20*, 2203–2226. [CrossRef]
6. Kori, J. Pratibha Effect of periodic permeability of lung airways on the flow dynamics of viscous fluid. *Nanosyst. Phys. Chem. Math.* **2019**, *10*, 235–242. [CrossRef]
7. Kori, J. Pratibha Numerical Simulation of Dusty Air Flow and Particle Deposition Inside Permeable Alveolar Duct. *Int. J. Appl. Comput. Math.* **2019**, *5*, 17. [CrossRef]
8. Pratibha, K.J. Simulation and Modeling for Aging and Particle Shape Effect on Airflow Dynamics and Filtration Efficiency of Human Lung. *J. Appl. Fluid Mech.* **2019**, *12*, 1273–1285.
9. Krishna, M.V.; Swarnalathamma, B.; Prakash, J. Heat and Mass Transfer on Unsteady MHD Oscillatory Flow of Blood Through Porous Arteriole. In *Applications of Fluid Dynamics. Lecture Notes in Mechanical Engineering*; Singh, M., Kushvah, B., Seth, G., Prakash, J., Eds.; Springer: Berlin/Heidelberg, Germany, 2017; pp. 207–224. [CrossRef]
10. Akbar, N.; Tripathi, D.; Khan, Z.; Bég, O.A. Mathematical modelling of pressure-driven micropolar biological flow due to metachronal wave propulsion of beating cilia. *Math. Biosci.* **2018**, *301*, 121–128. [CrossRef]
11. Ma, Z.; Li, B.; Peng, J.; Gao, D. Recent Development of Drug Delivery Systems through Microfluidics: From Synthesis to Evaluation. *Pharmaceutics* **2022**, *14*, 434. [CrossRef]
12. Nazeer, M.; Hussain, F.; Hameed, M.; Khan, M.I.; Ahmad, F.; Malik, M.; Shi, Q.-H. Development of mathematical modeling of multi-phase flow of Casson rheological fluid: Theoretical approach. *Chaos Solitons Fractals* **2021**, *150*, 111198. [CrossRef]
13. Ramesh, K.; Tripathi, D.; Bég, O.A. Cilia-assisted hydromagnetic pumping of biorheological couple stress fluids. *Propuls. Power Res.* **2019**, *8*, 221–233. [CrossRef]

14. Sedaghat, M.H.; Bagheri, A.A.H.; Shahmardan, M.M.; Norouzi, M.; Khoo, B.C.; Jayathilake, P.G. A Hybrid Immersed Boundary-Lattice Boltzmann Method for Simulation of Viscoelastic Fluid Flows Interaction with Complex Boundaries. *Commun. Comput. Phys.* **2021**, *29*, 1411–1445. [CrossRef]
15. Munawar, S.; Saleem, N. Entropy Analysis of an MHD Synthetic Cilia Assisted Transport in a Microchannel Enclosure with Velocity and Thermal Slippage Effects. *Coatings* **2020**, *10*, 414. [CrossRef]
16. Nazeer, M.; Hussain, F.; Ahmad, F.; Iftikhar, S.; Subia, G.S. Theoretical study of an unsteady ciliary hemodynamic fluid flow subject to the Newton's boundary conditions. *Adv. Mech. Eng.* **2021**, *13*, 16878140211040462. [CrossRef]
17. Su, M.; Mandal, M.S.; Mukhopadhyay, S. Numerical Simulation of Mass Transfer in Pulsatile Flow of Blood Characterized by Carreau Model under Stenotic Condition. *J. Appl. Fluid Mech.* **2021**, *14*, 805–817. [CrossRef]
18. Sangita, R.; Ranjeeta, B.; Bég, O.; Pradeep, B.; Ben, H. Pulsatile dissipative magne-to-bio-rheological fluid flow and heat transfer in a non-Darcy porous medium channel: Finite element modeling. *Emir. J. Eng. Res.* **2009**, *14*, 77–90.
19. Coppolo, D.P.; Schloss, J.; Suggett, J.A.; Mitchell, J.P. Non-Pharmaceutical Techniques for Obstructive Airway Clearance Focusing on the Role of Oscillating Positive Expiratory Pressure (OPEP): A Narrative Review. *Pulm. Ther.* **2022**, *8*, 1–41. [CrossRef]
20. Kirtane, A.R.; Verma, M.; Karandikar, P.; Furin, J.; Langer, R.; Traverso, G. Nanotechnology approaches for global infectious diseases. *Nat. Nanotechnol.* **2021**, *16*, 369–384. [CrossRef]
21. Singh, A.V.; Maharjan, R.S.; Kromer, C.; Laux, P.; Luch, A.; Vats, T.; Chandrasekar, V.; Dakua, S.P.; Park, B.-W. Advances in Smoking Related In Vitro Inhalation Toxicology: A Perspective Case of Challenges and Opportunities from Progresses in Lung-on-Chip Technologies. *Chem. Res. Toxicol.* **2021**, *34*, 1984–2002. [CrossRef]
22. Thiyagarajan, P.; Sathiamoorthy, S.; Santra, S.S.; Ali, R.; Govindan, V.; Noeiaghdam, S.; Nieto, J.J. Free and Forced Convective Flow in Pleural Fluid with Effect of Injection between Different Permeable Regions. *Coatings* **2021**, *11*, 1313. [CrossRef]
23. Hetnarski, R. On inverting the Laplace transforms connected with the error function. *Appl. Math.* **1964**, *7*, 399–405. [CrossRef]
24. Rehman, K.U.; Shatanawi, W.; Malik, M. Heat transfer and double sampling of stratification phenomena in non-Newtonian liquid suspension: A comparative thermal analysis. *Case Stud. Therm. Eng.* **2022**, *33*, 101934. [CrossRef]
25. Sindhu, T.N.; Hussain, Z.; Alotaibi, N.; Muhammad, T. Estimation method of mixture distribution and modeling of COVID-19 pandemic. *AIMS Math.* **2022**, *7*, 9926–9956. [CrossRef]
26. Shafiq, A.; Sindhu, T.N.; Alotaibi, N. A novel extended model with versatile shaped failure rate: Statistical inference with COVID -19 applications. *Results Phys.* **2022**, *36*, 105398. [CrossRef] [PubMed]
27. Enault, S.; Lombardi, D.; Poncet, P.; Thiriet, M. Mucus dynamics subject to air and wall motion. *ESAIM Proc. EDP Sci.* **2010**, *30*, 125–141. [CrossRef]